# Qudit-native measurement protocol for dynamical correlations using Hadamard tests

Pavel P. Popov,[1, *] Kevin T. Geier,[2, 3, 4] Valentin Kasper,[5] Maciej Lewenstein,[1, 6] and Philipp Hauke[2, 3]

[1]*ICFO - Institut de Ciencies Fotoniques, The Barcelona Institute of Science and Technology,*
*Av. Carl Friedrich Gauss 3, 08860 Castelldefels (Barcelona), Spain*
[2]*Pitaevskii BEC Center, CNR-INO and Dipartimento di Fisica, Università di Trento, 38123 Trento, Italy*
[3]*Trento Institute for Fundamental Physics and Applications, INFN, 38123 Trento, Italy*
[4]*Quantum Research Center, Technology Innovation Institute,*
*P.O. Box 9639, Abu Dhabi, United Arab Emirates*
[5]*Kipu Quantum GmbH, Greifswalderstr. 226, 10405 Berlin, Germany*
[6]*ICREA, Pg. Lluis Companys 23, 08010 Barcelona, Spain*
(Dated: April 7, 2025)

Dynamical correlations reveal important out-of-equilibrium properties of the underlying quantum many-body system, yet they are notoriously difficult to measure in experiments. While measurement protocols for dynamical correlations based on Hadamard tests for qubit quantum devices exist, they do not straightforwardly extend to qudits. Here, we propose a modified protocol to overcome this limitation by decomposing qudit observables into unitary operations that can be implemented and probed in a quantum circuit. We benchmark our algorithm numerically at the example of quench dynamics in a spin-1 XXZ chain with finite shot noise and demonstrate advantages in terms of signal-to-noise ratio over established protocols based on linear response. Our scheme can readily be implemented on various platforms and offers a wide range of applications like variational quantum optimization and probing thermalization in many-body systems.

## I. INTRODUCTION

The basic unit in which information is encoded in quantum computers is typically the qubit, the quantum generalisation of the classical bit. However, many physical systems naturally offer units with a higher-dimensional local Hilbert space. Embracing these higher dimensions leads to new ways for processing information based on qudits [1], with applications like alternative quantum algorithms [2], optimal measurements [3], and native encoding of complex quantum systems with higher local degrees of freedom [4]. On a fundamental level, the different coherence [5], dissipation, and entanglement structure [6] of qudit systems with respect to qubits can offer advantages for noise resilience [7] and quantum error correction [8]. Thanks to these favorable properties, qudits have gained traction on various quantum technology platforms [9–11] with manifold applications, e.g., in quantum cryptography [12, 13] and quantum simulation [14–16].

However, the new possibilities offered by qudit systems often come at the price of an increased complexity, such that not all quantum algorithms or measurement schemes generalize to qudits in a straightforward way. This calls for the design of novel protocols tailored specifically for qudit systems. Dynamical correlations involving observables at unequal times represent a class of observables that is inherently difficult to measure in quantum systems due to the collapse of the wave function. These quantities play a fundamental role in statistical mechanics. For example, they can be used to probe thermalization in isolated quantum systems via the so-called fluctuation–dissipation relation (FDR) [17–25] and thus provide a test of the eigenstate thermalization hypothesis (ETH) [26–34]. Furthermore, in the context of variational quantum algorithms [35, 36], many relevant observables like the gradient of the energy or the Fubini–Studi metric tensor [37] can be cast in the form of a dynamical correlation function [38–41]. Various protocols exist for measuring dynamical correlations, but they are often efficient only for certain platforms, types of observables, and measurement precision [24, 25, 42–46]. On digital qubit systems, the Hadamard-test [47] has proven to be a versatile and robust method for accessing dynamical correlations [38, 39, 48–53]. However, these protocols strongly rely on the fact that Pauli operators on qubits are both Hermitian and unitary, which is not the case for qudits.

In this work, we formulate the Hadamard-test procedure for qudit systems on deterministic quantum circuits, enabling measurements of dynamical correlation functions in many-body systems with a higher-dimensional local Hilbert space. This is achieved by decomposing dynamical correlation functions of arbitrary observables into sums of unitaries, which can be measured with Hadamard tests on the quantum device, requiring only a single ancillary qubit. We numerically test the performance of our protocol by simulating a measurement of the two-time commutator and anti-commutator in a spin-1 XXZ chain with finite shot noise, where our scheme proves to be more efficient than established linear-response-based techniques [18, 19]. Our measurement protocol can readily be implemented on various qudit quantum devices, e.g., based on trapped ions, superconducting circuits, or neutral atoms, and thus provides a versatile tool for characterizing many-body physics on

these platforms.

This paper is organized as follows. In Section II, we present the general measurement protocol in a platform-agnostic framework. Section III puts forward our numerical results illustrating the Hadamard-test protocol for measuring dynamical correlations in a spin-1 XXZ chain with finite shot noise, followed by a comparison to linear-response-based schemes and a discussion of perspectives for an experimental realization. Finally, we present our conclusions in Section IV.

## II. MEASUREMENT PROTOCOL

Our goal is to measure dynamical correlation functions of two Hermitian (multi-)qudit observables $\hat{A}$ and $\hat{B}$ of the form

$$C_{AB}(t_1, t_2) = \langle \hat{A}(t_1)\hat{B}(t_2) \rangle, \tag{1}$$

where we use the shorthand notation $\hat{O}(t) = \hat{U}^\dagger(t)\hat{O}\hat{U}(t)$. The unitary operator $\hat{U}(t)$ may equally well describe a Hamiltonian time evolution (e.g., in cold-atom experiments) or a sequence of quantum gates on a digital quantum device, for example, representing a parametrized quantum circuit in the context of variational quantum simulation algorithms [38]. In general, the two-time correlator in Eq. (1) is a complex-valued quantity, $C_{AB} = C_{AB}^+/2 - iC_{AB}^-/2$, whose real and imaginary parts are given, respectively, by the two-time anti-commutator

$$C_{AB}^+(t_1, t_2) = \langle \{ \hat{A}(t_1), \hat{B}(t_2) \} \rangle \tag{2a}$$

and commutator

$$C_{AB}^-(t_1, t_2) = i\langle [ \hat{A}(t_1), \hat{B}(t_2) ] \rangle. \tag{2b}$$

Figure 1 illustrates the quantum circuit implementing the measurement protocol for dynamical correlations. The qudit register representing the physical system of interest is initialized in the state $|\psi_0\rangle$. Its evolution under the operator $\hat{U}(t)$ is interrupted at the times $t_1$ and $t_2$ by controlled gates coupling the register to an ancillary qubit. These gates represent the action of observables $\hat{A}$ and $\hat{B}$, whose dynamical correlation we intend to measure. The value of the corresponding correlation function is obtained by measuring the probability of the ancillary qubit to be in the computational $|0\rangle$ state at the end of the circuit. So far, the protocol corresponds to the standard Hadamard-test procedure well-known for qubits [38], which strongly relies on the fact that observables are both Hermitian and unitary. By contrast, for qudits, operators $\hat{A}$ and $\hat{B}$ are typically not unitary and therefore do not directly correspond to physical quantum gates.

In order to extend such a protocol to qudits, we represent $\hat{A}$ and $\hat{B}$ as a sum of unitary operations that can be inserted in the quantum circuit. The procedure can be seen as a special case of the more general linear combination of unitaries (LCU) method [54]. In general, we can decompose a Hermitian qudit operator $\hat{X}$ into a sum of a unitary operator $\hat{W}_X$ and its Hermitian conjugate as

$$\hat{X} = \frac{1}{2}\|\hat{X}\|(\hat{W}_X + \hat{W}_X^\dagger), \tag{3}$$

where $\|\cdot\|$ denotes the spectral norm of the operator (given by the eigenvalue with the largest magnitude). The above relation can readily be inverted, yielding

$$\hat{W}_X = \frac{\hat{X}}{\|\hat{X}\|} + i\sqrt{\mathbb{1} - \frac{\hat{X}^2}{\|\hat{X}\|^2}}. \tag{4}$$

This decomposition allows us to rewrite Eq. (1) as a sum of correlation functions of unitaries,

$$C_{AB}(t_1, t_2) = \frac{1}{4}\|\hat{A}\|\|\hat{B}\| \sum_{V,V' \in \{W, W^\dagger\}} C_{V_A V_B'}(t_1, t_2). \tag{5}$$

The real and imaginary parts of the correlators appearing on the right-hand side of Eq. (5) can now be accessed by distinct realizations of the circuit in Fig. 1, where the controlled gates correspond to the unitaries $\hat{W}_A^{(\dagger)}$ and $\hat{W}_B^{(\dagger)}$. Let $|\Psi_{V_A V_B}^\pm(t_1, t_2)\rangle$ be the total quantum state after execution of the circuit, given the initial ancilla state $|\phi_0^\pm\rangle = (|0\rangle + e^{i\alpha_\pm}|1\rangle)/\sqrt{2}$ with $\alpha_+ = 0$ and $\alpha_- = \pi/2$ and intermittent controlled unitaries $\hat{V}_A \in \{\hat{W}_A, \hat{W}_A^\dagger\}$ and $\hat{V}_B \in \{\hat{W}_B, \hat{W}_B^\dagger\}$. As shown in Appendix A, the value of the two-time (anti-)commutator can be extracted from the probability $P_{V_A V_B}^\pm(t_1, t_2) = |\langle 0|\Psi_{V_A V_B}^\pm(t_1, t_2)\rangle|^2$ of measuring the ancillary qubit in the state $|0\rangle$ according to

$$C_{AB}^\pm(t_1, t_2) = \|\hat{A}\|\|\hat{B}\| \sum_{V,V' \in \{W, W^\dagger\}} \left( P_{V_A V_B'}^\pm(t_1, t_2) - \frac{1}{2} \right). \tag{6}$$

Therefore, the same circuit allows one to measure either the real or the imaginary part of the dynamical correlation function simply by preparing the ancillary qubit in a different initial state.

A quantity of practical importance is the variance of the estimator for the dynamical correlation function in Eq. (5), as it determines the number of measurements that need to be performed on the quantum device to obtain $C_{AB}^\pm$ with sufficient precision. ~~In Appendix B, we derive the result~~ If the probabilities $P_{V_A V_B}^\pm$ are estimated by repeating the Hadamard test with controlled unitaries $\hat{V}_A$ and $\hat{V}_B$, respectively, $M_{V_A V_B}$ times, the two-time (anti-)commutator can be estimated with variance

$$\mathrm{Var}[C_{AB}^\pm] = \|\hat{A}\|^2 \|\hat{B}\|^2 \sum_{V,V' \in \{W, W^\dagger\}} \frac{P_{V_A V_B'}^\pm (1 - P_{V_A V_B'}^\pm)}{M_{V_A V_B'}}. \tag{7}$$

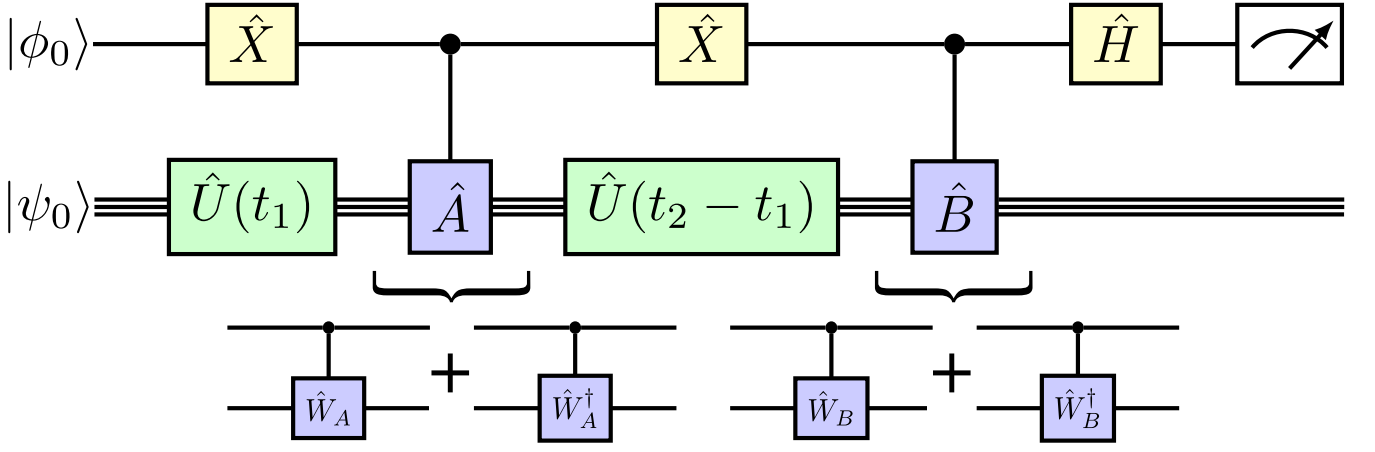The derivation of this result is reported Appendix B. Although the precise value of the variance ultimately

FIG. 1. **Quantum circuit for measuring dynamical correlations based on Hadamard tests, extended to qudit devices.** The general structure consists of a qudit register that implements the physical system of interest plus an ancillary qubit. The register is initialized in state $|\psi_0\rangle$ and evolves under the unitary time-evolution operator $\hat{U}(t)$. The ancilla is subject to bit flip gates $\hat{X}$ and the Hadamard gate $\hat{H}$. In order to obtain the real and the imaginary parts of the dynamical correlation $\langle \hat{A}(t_1)\hat{B}(t_2)\rangle$, the ancillary qubit is initialized in the state $|\phi_0^{\pm}\rangle = (|0\rangle + e^{i\alpha_{\pm}}|1\rangle)/\sqrt{2}$ with $\alpha_+ = 0$ and $\alpha_- = \pi/2$, respectively. The decomposition of the qudit observables $\hat{A}$ and $\hat{B}$ into a sum of two unitaries $\hat{W}_X$ and $\hat{W}_X^{\dagger}$ with $X \in \{A, B\}$, makes it possible to implement their action as controlled quantum gates between the ancilla and the register. After the circuit is executed, measuring the probability of finding the ancilla in the state $|0\rangle$ gives access to the desired value of the dynamical correlation function.

depends on the details of the system, a useful *a priori* upper bound is given by the product of the square norms of observables $\hat{A}$ and $\hat{B}$, $\mathrm{Var}[C_{AB}^{\pm}] \leq M^{-1}\|\hat{A}\|^2\|\hat{B}\|^2$, assuming $M$ shots are allocated for measuring each configuration. This result is consistent with the bound on the variance directly derivable from Eq. (2) for a (hypothetical) projective measurement of the (anti-)commutator with a total budget of $4M$ shots, $\mathrm{Var}[C_{AB}^{\pm}] \leq (4M)^{-1}4\|\hat{A}\|^2\|\hat{B}\|^2$.

In what follows, we illustrate our protocol for measuring dynamical correlations using numerical simulations and benchmark its performance with finite measurement statistics.

## III. NUMERICAL RESULTS

In this section, we illustrate our protocol via numerical simulations for the example of quench dynamics in a spin-1 XXZ chain. This model represents a natural extension to qudit systems from its spin-1/2 version, which has served as a paradigmatic platform for testing novel quantum algorithms on qubit-based quantum hardware in the context of many-body quantum simulations [55]. Notably, closely related spin-1 models have been implemented on recently developed qudit quantum processors [56], representing promising targets for our proposed protocol. Furthermore, the spin-1 XXZ chain exhibits a richer phase diagram than its spin-1/2 counterpart, including the emergence of topological phases [57–59]. These properties make the model appealing for demonstrating and validating our qudit-native approach

for measuring dynamical correlations.

Apart from statistical errors, our protocol is exact in the sense that it does not involve approximations that could lead to systematic errors. This is in contrast to protocols based on linear response, where by design a trade-off between accuracy and signal-to-noise ratio has to be made. We therefore benchmark our technique for measuring dynamical correlations based on Hadamard tests with a particular focus on its performance in a finite-statistics setting compared to linear-response measurements.

### A. Quench dynamics in a spin-1 XXZ chain

We consider an XXZ chain of $N$ spin-1 particles, whose Hamiltonian is given by

$$\hat{H} = \sum_{i=1}^{N-1}\left[ J_{xy}\left(\hat{S}_i^x \hat{S}_{i+1}^x + \hat{S}_i^y \hat{S}_{i+1}^y\right) + J_z \hat{S}_i^z \hat{S}_{i+1}^z\right]. \quad (8)$$

Here, $\hat{S}_i^{\alpha}$, with $\alpha \in \{x, y, z\}$, are spin-1 matrices acting on spin $i$, while $J_{xy}$ and $J_z$ denote the interaction strengths in the $xy$-plane and in $z$-direction, respectively. In order to initiate quench dynamics, we prepare the system deeply in the antiferromagnetic Néel phase, corresponding to the ground state for $J_z/J_{xy} \to \infty$. Since the ground state is degenerate in this limit, we choose a $\mathbb{Z}_2$-symmetric superposition of the two Néel states, but this choice is not crucial for our purposes. The system is then evolved under the Hamiltonian (8) with $J_z/J_{xy} = 0.5$,
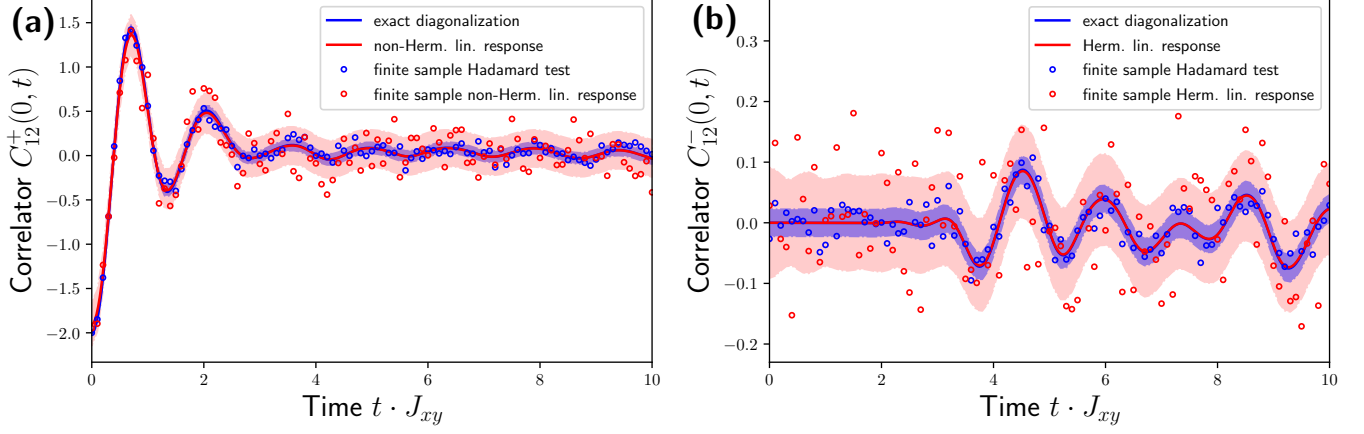
FIG. 2. **Dynamical correlation functions after a quench in the spin-1 XXZ chain model.** The system of $N = 10$ spins is initialized in the equal superposition of the two degenerate ground states of the model for $J_z/J_{xy} \to \infty$ and, after the quench, undergoes unitary evolution under the Hamiltonian $H_0$ with $J_z/J_{xy} = 0.5$. The solid lines show the time trace of the two-time (a) anti-commutator and (b) commutator for the Hadamard-test protocol (blue) and for the linear-response protocol (red) with perturbation strength $\lambda = 0.2$ and a pulse area $J_{xy}\Delta t = 10^{-3}$. The shaded areas mark the standard error of the mean computed directly from the quantum state, while the colored circles correspond to the expectation values obtained from sampling with finite statistics, illustrating the effect of shot noise. The Hadamard-test measurement of the anti-commutator (commutator) was sampled with 1500 (8000) shots per point, whereas the sampled linear-response measurement corresponds to 1500 (12000) shots per point. For a comparable total budget of shots, the Hadamard-test protocol achieves a better signal-to-noise ratio than the linear-response protocol throughout the simulation.

which on the phase diagram lies in the bulk of the so-called Haldane phase [59]. While the initial state is characterized by antiferromagnetic order, which exhibits non-decaying spin–spin correlations, the Haldane phase is a gapped topological phase, characterized by non-vanishing string correlations. Moreover, it is considered a disordered phase; i.e., spin–spin correlations decay exponentially. Therefore, quenching from the antiferromagnetic phase to the Haldane phase, we expect to observe non-trivial dynamics in the two-point dynamical spin–spin correlations.

Specifically, we are interested in extracting the dynamical correlation functions in Eq. (2) for the $\hat{S}^z$ operator of two distinct spins $i$ and $j$ in the chain, denoted by $C_{ij}^{\pm}(t_1, t_2) \equiv C_{S_i^z S_j^z}^{\pm}(t_1, t_2)$. Following standard conventions [60], we consider only the "connected part" of the two-time anti-commutator, $C_{ij}^+(t_1, t_2) \to C_{ij}^+(t_1, t_2) - 2\langle \hat{S}_i^z(t_1)\rangle\langle \hat{S}_j^z(t_2)\rangle$ (the product of expectation values forming the "disconnected part" can be obtained from standard projective measurements). In Fig. 2, we show the time trace of the two-time (anti-)commutator $C_{12}^{\pm}(0, t)$ after the quench.

## B. Hadamard-test protocol with finite measurement statistics

In this section, we investigate how well our Hadamard-test protocol reproduces the above ideal results with finite statistics.

### 1. Implementation of the controlled unitaries for spin observables

In order to implement our protocol, we need to calculate the explicit form of the unitary operators in the decomposition of Eq. (3). While for a general qudit observable $\hat{X}$ the structure of the resulting unitary $\hat{W}_X$ may be complicated, the situation simplifies for spin observables. The relevant operator for our case study is the single-spin $\hat{S}_z$ operator. In the general spin-$S$ case, the matrix elements with respect to the eigenbasis of the $\hat{S}_z$ operator take the simple form

$$\langle m \,|\, \hat{W}_{S_z} \,|\, m'\rangle = \delta_{m,m'}\left(\frac{m}{S} + i\sqrt{1 - \frac{m^2}{S^2}}\right), \quad (9)$$

where $m, m' \in \{S, \ldots, -S\}$. In particular, for $S = 1$, we find in matrix representation

$$\hat{S}^z = \begin{pmatrix} 1 & 0 & 0 \\ 0 & 0 & 0 \\ 0 & 0 & -1 \end{pmatrix} \quad \Rightarrow \quad \hat{W}_{S_z} = \begin{pmatrix} 1 & 0 & 0 \\ 0 & i & 0 \\ 0 & 0 & -1 \end{pmatrix}. \quad (10)$$

The unitaries $\hat{W}_{S_x}$ and $\hat{W}_{S_y}$ can be obtained by applying the basis change that transforms $\hat{S}^x$ and $\hat{S}^y$ to $\hat{S}^z$, respectively. We note that the controlled phase gate represented by $\hat{W}_z$ is generally available on state-of-the-art qudit quantum devices, in some cases even as a native operation [61]. Furthermore, for any many-body spin observable $\hat{X}$, we can calculate $W_{\hat{X}}$ explicitly by using the

representation of $\hat{X}$ as a sum of spin operator strings, as shown in Appendix C.

### 2. Performance benchmark in the presence of shot noise

In an experimental setting, the expectation values in Eq. (11) as well as the outcome of the Hadamard tests are subject to errors caused by finite measurement statistics. We simulate these shot-noise errors by sampling the observables from the ideal distribution given by the total wave function of the system–ancilla register after the execution of the Hadamard-test circuit. To this end, we assign a total budget of shots for measuring the four probabilities on the right-hand side of Eq. (6) as well as the two expectation values forming the disconnected part of the anti-commutator.

Figure 2 compares the exact value of $C_{12}^{\pm}(0,t)$ (blue solid line) to the one obtained from sampling with finite statistics (blue circles). The shot noise is low enough to allow for an accurate measurement of the two-time anti-commutator (commutator) already for a moderate number of 250 (2000) shots for each expectation value, resulting in a total of 1500 (8000) shots per point.

### C. Comparison to protocols based on linear response

In this section, we compare our Hadamard-test protocol with other protocols for measuring dynamical correlation functions. Many such protocols are specific to certain platforms or observables. To keep our analysis general, we focus the following discussion on protocols based on linear response theory [18, 19]. In fact, a large class of well-established protocols for measuring dynamical correlations, including non-invasive (or weak) measurements [44], can be phrased in an implementation-independent way using this framework [25].

#### 1. (Non-)Hermitian linear-response protocol

As well known in linear response theory, the response of the system to a weak (Hermitian) perturbation gives access to the two-time *commutator* according to Kubo's formula [18, 19]. More recently, measuring the two-time *anti-commutator* by probing the linear response to a *non-Hermitian* perturbation was proposed [25, 62, 63]. Here, we employ such linear-response protocols to extract the response function directly in the time domain and benchmark the result against our Hadamard-test protocol.

Specifically, to measure the two-time (anti-)commutator $C_{ij}^{\pm}(t_1,t_2)$, the system is first evolved under the unperturbed Hamiltonian $\hat{H}_0$ to the time $t_1$. Then, a Hermitian (anti-Hermitian) perturbation of strength $0 < \lambda \ll 1$ by the operator $\hat{S}_j^z$ is applied in the form of a short rectangular pulse of duration $\Delta t$,

during which the system evolves under the perturbed Hamiltonian $\hat{H}_\lambda = \hat{H}_0 - \lambda\hbar J_{xy}\hat{S}_j^z$ (in the non-Hermitian case, we have $\lambda \to i\lambda$). After the perturbation is released, the system is evolved under the unperturbed Hamiltonian $\hat{H}_0$ up to time $t_2$, and the expectation value of the observable $\hat{S}_i^z$ is measured, yielding the two-time (anti-)commutator via

$$C_{ij,\,\mathrm{LR}}^{\pm}(t_1,t_2) = \frac{1}{\lambda J_{xy}\Delta t}\left[\langle \hat{S}_i^z(t_2)\rangle_{\pm} - \langle \hat{S}_i^z(t_2)\rangle\right]. \quad (11)$$

Here $\langle\cdots\rangle_{\pm}$ and $\langle\cdots\rangle$ denote expectation values with respect to the perturbed and unperturbed states, respectively. In the non-Hermitian case, we normalize the expectation value as $\langle\cdots\rangle_+ \to \langle\cdots\rangle_+/\langle\mathbb{1}\rangle_+$, accounting for the loss of probability to a complementary state space.

#### 2. Finite statistics and bias–variance trade-off

As depicted in Fig. 2, the linear-response protocol accurately reproduces the time trace of the dynamical correlations for a sufficiently weak perturbation and infinite measurement statistics (red solid line). An advantage of our Hadamard-test protocol over the linear-response method becomes apparent if one takes statistical errors due to shot noise into account. The red circles show the sampled values of the anti-commutator (commutator) using 750 (6000) shots for each expectation value in Eq. (11), corresponding to a total of 1500 (12000) shots per point, which is comparable to the total budget used for the Hadamard-test protocol [64]. One can see that the Hadamard-test protocol yields a lower statistical variance and therefore a higher signal-to-noise ratio.

In order to benchmark the relative performance of the Hadamard-test protocol and the linear-response protocol, we investigate the two figures of merit shown in Fig. 3: the relative error

$$\mathcal{R}_{ij}^{\pm} = \frac{\int_0^t dt'\,|C_{ij}^{\pm}(0,t') - C_{ij,\,\mathrm{LR}}^{\pm}(0,t')|^2}{\int_0^t dt'\,|C_{ij}^{\pm}(0,t')|^2}, \quad (12)$$

measuring the systematic error of the linear-response protocol due to non-linear effects, and the time average of the standard deviation,

$$\Delta C_{ij}^{\pm} = \frac{1}{t}\int_0^t dt'\,\Delta C_{ij}^{\pm}(0,t'), \quad (13)$$

measuring the statistical errors due to shot noise.

The linear-response protocol generally requires a trade-off between accuracy and signal-to-noise ratio. On the one hand, the perturbation should be sufficiently weak that the response is in the linear regime, where nonlinear contributions to the response are negligible. On the other hand, it should be sufficiently strong that the signal is resolvable against the background noise. As can be seen in Fig. 3, the error grows with increasing $\lambda$, while the variance shrinks and vice versa. This behavior can

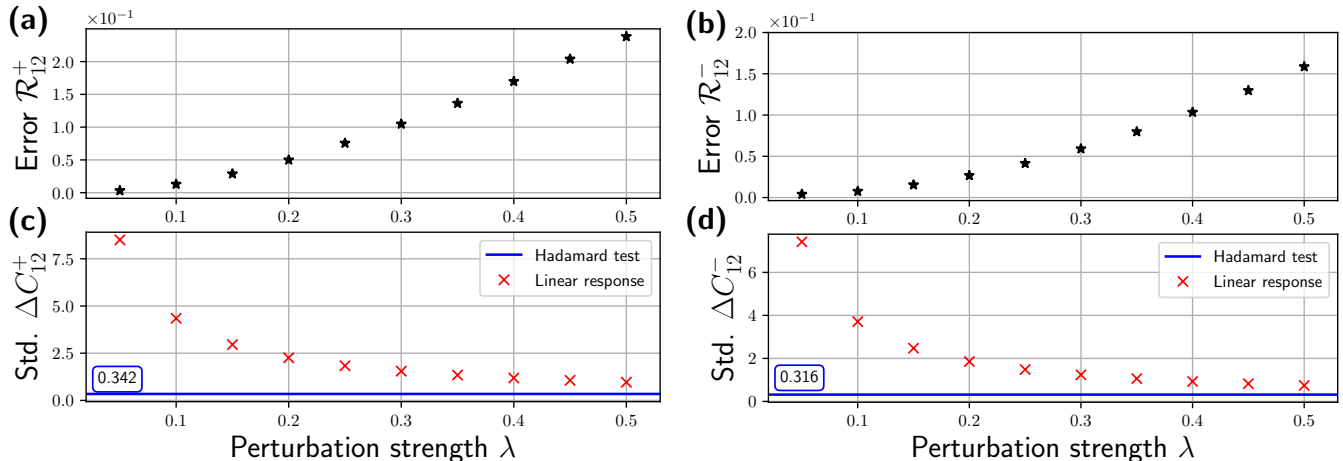FIG. 3.  **Bias–variance tradeoff in the linear-response measurement of dynamical correlations.** With increasing perturbation strength $\lambda$, the linear-response protocol incurs systematic errors in the two-time (a) anti-commutator and (b) commutator due to nonlinear effects. Concomitantly, the statistical error (standard deviation of a single measurement) of the (c) anti-commutator and (d) commutator decreases, requiring a trade-off between accuracy and signal-to-noise ratio. By contrast, the Hadamard-test protocol exhibits consistently lower statistical errors and does not introduce intrinsic systematic sources of error.

be viewed as a manifestation of the bias–variance tradeoff, which is well-known in statistics and machine learning. Importantly, there is no such trade-off in the case of our Hadamard-test protocol. Furthermore, in the investigated quench scenario, the Hadamard-test protocol outperforms the linear-response protocol both in terms of accuracy and signal-to-noise ratio.

### 3.  Experimental resources

A fair comparison between our Hadamard-test protocol and the linear-response protocol also requires a discussion of the experimental resources required for their implementation. In what follows, we discuss the cases of measuring the unequal-time commutator and anti-commutator separately.

For the commutator, the linear-response protocol requires a standard Hermitian perturbation, which either may be single-body, as in the case of spin–spin dynamical correlations, or may involve few-body interactions. Importantly, the protocol typically admits ancilla-free realizations, where the perturbation is exerted directly on the system, e.g., in the form of a rapid change in the couplings in the Hamiltonian or as a unitary gate in a quantum circuit. By contrast, the protocol based on Hadamard tests requires an ancillary qubit and two entangling operations between this qubit and the system. Thus, depending on the device and scenario at hand, a decision has to be made between additional errors from shot noise and bias (for the linear-response protocol; see Fig. 3) and potential errors from faulty gates (for the Hadamard-test protocol). One way of circumventing the

need for a physical ancilla for the Hadamard test is to use qudits with the number of controllable levels equal to double the local Hilbert space dimension of the system we want to simulate (e.g., $d = 6$ in the example above).

In our benchmarks of the anti-commutator, we have considered an implementation-agnostic "ideal" non-Hermitian linear-response measurement, where a non-Hermitian perturbation directly acts on the system degrees of freedom. However, physical realizations of this scenario typically incur additional experimental overhead, e.g., entangling the system with an ancilla and performing postselected measurements on the ancilla state [25]. Therefore, engineering an (approximate) effective non-Hermitian Hamiltonian requires resources similar to those of the Hadamard-test protocol.

Finally, we turn our attention to potential near-term experimental realizations of our Hadamard-test protocol for dynamical correlations of general observables. For systems with a large Hilbert space, implementing a general multi-qudit observable as a sum of unitaries presents significant practical challenges. While the decomposition in Eq. (3) applies to any observable, the resulting unitary may have a complicated structure (unlike for spin observables; see Section III B 1). In this case, the gate complexity may be reduced by resorting to approximate decompositions, e.g., based on the LCU procedure [54], where one can trade off lower circuit depth for a more accurate approximation. While in typical applications the circuit depth is dominated by the number of gates required to implement the system's time evolution, the added gate complexity due to the (approximate) implementation of the controlled unitaries may be of concern on noisy intermediate-scale quantum (NISQ) devices: In

the presence of circuit noise, the maximum circuit depth is restricted by the finite coherence time. This may require lowering the approximation accuracy of the controlled unitaries, introducing systematic errors, and it may impose limits on the times $t_1$ and $t_2$ of the dynamical correlations that can reliably be measured using the Hadamard test protocol. In situations where this effect is identified as a limiting factor, the linear-response protocol may provide a viable alternative since the implementation of the perturbation is typically favorable in terms of gate complexity.

## IV. CONCLUSION

In this work, we proposed an algorithm for measuring dynamical correlation functions on qudit quantum hardware. Key to the scheme is the decomposition of general (multi-)qudit observables into unitaries, which can be exploited to represent dynamical correlations as the sum of quantities accessible via Hadamard tests. We numerically benchmarked the performance of this protocol with finite measurement statistics using the example of a spin-1 XXZ model after a quench. Notably, in this scenario the Hadamard-test protocol outperforms established protocols based on linear response theory in terms of both accuracy and the number of shots needed to distinguish the signal from noise.

The Hadamard-test protocol for dynamical correlation functions can be extended in a straightforward way to measuring higher-order temporal correlations of the form $\langle A_1(t_1) \cdots A_n(t_n) \rangle$. Such a generalization of our protocol would require only the implementation of deeper circuits and a higher number of controlled operations, while the structure of the circuit and the usage of the decomposition of Hermitian operators into a sum of unitaries remain the same.

Finally, we emphasize that our Hadamard-test protocol for measuring dynamical correlations in qudit quantum systems can be used as a subroutine in existing algorithms with wide-ranging applications, ranging from thermalization in many-body systems [24, 25, 53, 65] to the implementation of variational optimization protocols for the simulation of equilibrium and non-equilibrium properties of many-body systems [36, 40, 41]. Moreover, the protocol is designed such that it can be implemented on presently available quantum simulation platforms, including trapped ions, cold atoms, and superconducting qubits.

## V. ACKNOWLEDGEMENTS

sity and Research. Neither the European Union nor the granting authority can be held responsible for them.

## Appendix A: Outcome of the quantum circuit implementing the Hadamard-test protocol

In this appendix, we derive Eq. (6) by calculating the state of the system after applying each quantum gate in Fig. 1. The system–ancilla register is initialized in the state

$$|\Psi_0^\alpha\rangle = \frac{1}{\sqrt{2}}(|0\rangle + e^{i\alpha}|1\rangle) \otimes |\psi_0\rangle \qquad (A1)$$

with $\alpha \in \{0, \frac{\pi}{2}\}$, depending on whether we want to measure the unequal-time anti-commutator or commutator. After flipping the ancilla, evolving the state up to time $t_1$, and applying the first controlled operation $\hat{V}_A$, we obtain the intermediate state

$$\frac{1}{\sqrt{2}}e^{i\alpha}|0\rangle \otimes \hat{U}(t_1)|\psi_0\rangle + \frac{1}{\sqrt{2}}|1\rangle \otimes \hat{V}_A\hat{U}(t_1)|\psi_0\rangle . \quad (A2)$$

Next, we apply the second ancilla flip, evolve the register up to time $t_2$, and apply the second controlled operation $\hat{V}_B$, yielding

$$\frac{1}{\sqrt{2}}|0\rangle \otimes \hat{U}(t_2 - t_1)\hat{V}_A\hat{U}(t_1)|\psi_0\rangle$$
$$+\frac{1}{\sqrt{2}}e^{i\alpha}|1\rangle \otimes \hat{V}_B\hat{U}(t_2)|\psi_0\rangle . \qquad (A3)$$

Finally, after performing the basis transformation on the ancilla via the Hadamard gate, the final state before the measurement reads

$$|\Psi_{V_A V_B}^\alpha(t_1,t_2)\rangle$$
$$=|0\rangle \otimes \left[\frac{1}{2}\hat{U}(t_2-t_1)\hat{V}_A\hat{U}(t_1)|\psi_0\rangle + \frac{1}{2}e^{i\alpha}\hat{V}_B\hat{U}(t_2)|\psi_0\rangle\right]$$
$$+|1\rangle \otimes \left[\frac{1}{2}\hat{U}(t_2-t_1)\hat{V}_A U(t_1)|\psi_0\rangle - \frac{1}{2}e^{i\alpha}\hat{V}_B\hat{U}(t_2)|\psi_0\rangle\right] . \qquad (A4)$$

The probability for the ancillary qubit to be in the computational state $|0\rangle$ is therefore given by

$$2\big|\langle 0|\Psi_{V_A V_B}^\alpha(t_1,t_2)\rangle\big|^2 - 1$$
$$= \frac{1}{2}e^{-i\alpha}\langle\psi_0|\hat{U}^\dagger(t_2)\hat{V}_B^\dagger\hat{U}(t_2-t_1)\hat{V}_A\hat{U}(t_1)|\psi_0\rangle + \text{c.c.} , \qquad (A5)$$

where c.c. denotes the complex conjugate. By setting $\alpha = \alpha_+ := 0$ and $\alpha = \alpha_- := \pi/2$, we get the real and the imaginary parts of the dynamical correlation function of $\hat{V}_A$ and $\hat{V}_B^\dagger$, respectively:

$$2P_{V_A V_B}^+(t_1,t_2) - 1 = \frac{1}{2}\langle \hat{V}_A^\dagger(t_1)\hat{V}_B(t_2) + \hat{V}_B^\dagger(t_2)\hat{V}_A(t_1)\rangle$$
$$= \text{Re}\langle \hat{V}_B^\dagger(t_2)\hat{V}_A(t_1)\rangle , \qquad (A6a)$$
$$2P_{V_A V_B}^-(t_1,t_2) - 1 = \frac{1}{2}i\langle \hat{V}_A^\dagger(t_1)\hat{V}_B(t_2) - \hat{V}_B^\dagger(t_2)\hat{V}_A(t_1)\rangle$$
$$= \text{Im}\langle \hat{V}_B^\dagger(t_2)\hat{V}_A(t_1)\rangle . \qquad (A6b)$$

By means of the decomposition in Eq. (5), we can express the two-time (anti-)commutator as

$$C_{AB}^\pm = \frac{1}{4}\|\hat{A}\|\|\hat{B}\| \sum_{V,V'\in\{W,W^\dagger\}} \langle e^{i\alpha_\pm}\hat{V}_A\hat{V}_B' + e^{-i\alpha_\pm}\hat{V}_B'\hat{V}_A\rangle$$
$$= \frac{1}{4}\|\hat{A}\|\|\hat{B}\| \sum_{V,V'\in\{W,W^\dagger\}} \langle e^{-i\alpha_\pm}\hat{V}_B'^\dagger\hat{V}_A + e^{i\alpha_\pm}\hat{V}_A^\dagger\hat{V}_B'\rangle$$
$$= \frac{1}{2}\|\hat{A}\|\|\hat{B}\| \sum_{V,V'\in\{W,W^\dagger\}} \big(\text{Re}\langle\hat{V}_B'^\dagger\hat{V}_A\rangle\cos\alpha_\pm$$
$$+ \text{Im}\langle\hat{V}_B'^\dagger\hat{V}_A\rangle\sin\alpha_\pm\big) , \qquad (A7)$$

where in the second line we have rearranged the terms in the sum. Combining this expression with Eq. (A6) finally yields the desired result in Eq. (6).

## Appendix B: Variance of the Hadamard test

We proceed with the proof of Eq. (7). To this end, we rewrite Eq. (6) by expressing the probability $P_{V_A V_B}^\pm(t_1,t_2)$ of measuring $|0\rangle$ on the ancilla as the expectation value of the projector $\hat{\Pi}_0 = |0\rangle\langle 0| \otimes \mathbb{1}$:

$$C_{AB}^\pm(t_1,t_2) = \|\hat{A}\|\|\hat{B}\|$$
$$\times \sum_{V,V'\in\{W,W^\dagger\}} \left(\langle \Psi_{V_A V_B'}^\pm(t_1,t_2)|\hat{\Pi}_0|\Psi_{V_A V_B'}^\pm(t_1,t_2)\rangle - \frac{1}{2}\right). \quad (B1)$$

Since the measurements of the four Hadamard-test configurations with controlled unitaries $\hat{V}_A \in \{\hat{W}_A, \hat{W}_A^\dagger\}$ and $\hat{V}_B \in \{\hat{W}_B, \hat{W}_B^\dagger\}$ are independent, standard propagation of variance yields [67]

$$\text{Var}[C_{AB}^\pm(t_1,t_2)] = \|\hat{A}\|^2\|\hat{B}\|^2 \sum_{V,V'\in\{W,W^\dagger\}} \text{Var}[\hat{\Pi}_0]_{V_A V_B'}^\pm(t_1,t_2) . \qquad (B2)$$

If the Hadamard test with controlled unitaries $\hat{V}_A$ and $\hat{V}_B$ is repeated $M_{V_A V_B}$ times, the probability $P_{V_A V_B}^\pm(t_1,t_2)$

can be estimated with variance

$$
\begin{aligned}
\mathrm{Var}[\hat{\Pi}_0]^{\pm}_{V_A V_B}&(t_1,t_2) \\
= \frac{1}{M_{V_A V_B}} &\Big[\left\langle \Psi^{\pm}_{V_A V_B}(t_1,t_2)\,\big|\,\hat{\Pi}_0^2\,\big|\,\Psi^{\pm}_{V_A V_B}(t_1,t_2)\right\rangle \\
&- \left\langle \Psi^{\pm}_{V_A V_B}(t_1,t_2)\,\big|\,\hat{\Pi}_0\,\big|\,\Psi^{\pm}_{V_A V_B}(t_1,t_2)\right\rangle^2\Big].
\end{aligned}
\tag{B3}
$$

For the projector $\hat{\Pi}_0$, the simple identity $\hat{\Pi}_0^2 = \hat{\Pi}_0$ holds, and thus for an arbitrary state

$$
\langle\hat{\Pi}_0^2\rangle - \langle\hat{\Pi}_0\rangle^2 = \langle\hat{\Pi}_0\rangle\big(1 - \langle\hat{\Pi}_0\rangle\big).
\tag{B4}
$$

Finally, identifying the expectation value $\langle\hat{\Pi}_0\rangle$ with the probability $P^{\pm}_{V_A V_B}(t_1,t_2)$ concludes the proof.

In order to arrive from Eq. (7) at the *a priori* upper bound $\mathrm{Var}[C^{\pm}_{AB}(t_1,t_2)] \leq M^{-1}\|\hat{A}\|^2\|\hat{B}\|^2$, we used the fact that the function $f(x) = x(1-x)$ has a maximum value $f(x=1/2) = 1/4$ in the interval $[0,1]$.

### Appendix C: Decomposition for many-body observables

Typical $n$-spin observables are given by strings of the form

$$
\hat{X} = \hat{S}_1^{\alpha_1} \otimes \cdots \otimes \hat{S}_n^{\alpha_n},
\tag{C1}
$$

where each $\hat{S}_k^{\alpha_k}$, with $\alpha_k \in \{x,y,z\}$, is a spin operator. The unitary $\hat{W}_X$ can then be calculated using the unitary decomposition of each of the (one-body) spin operators:

$$
\hat{S}_k^{\alpha_k} = \frac{1}{2}\|\hat{S}_k^{\alpha_k}\|(\hat{W}_{\alpha_k} + \hat{W}_{\alpha_k}^{\dagger}).
\tag{C2}
$$

Inserting Eq. (C2) into Eq. (C1) and using the definition of $\hat{W}_X$, we get

$$
\hat{W}_X = \sum_{\left\{V_k = W_{\alpha_k}, W_{\alpha_k}^{\dagger}\right\}} \hat{V}_1 \otimes \cdots \otimes \hat{V}_n.
\tag{C3}
$$

In this case, the experimental implementation of the controlled unitaries in the Hadamard-test simplifies since we have to deal with only a product of two-body operations. However, the number of Hadamard tests to be performed increases exponentially with the length of the string in Eq. (C1).

For a general multi-qudit observable, representations similar to strings of one-qudit observables can be employed to simplify the experimental implementation of controlled operations in the Hadamard test. In practice, however, an approximate decomposition such as the one resulting from the LCU procedure [54] may be more efficient in terms of circuit depth for implementations on NISQ devices.

[1] Y. Wang, Z. Hu, B. C. Sanders, and S. Kais, Qudits and high-dimensional quantum computing, Front. Phys. **8**, 479 (2020).

[2] B. P. Lanyon, M. Barbieri, M. P. Almeida, T. Jennewein, T. C. Ralph, K. J. Resch, G. J. Pryde, J. L. O'Brien, A. Gilchrist, and A. G. White, Simplifying quantum logic using higher-dimensional Hilbert spaces, Nat. Phys. **5**, 134 (2008).

[3] R. Stricker, M. Meth, L. Postler, C. Edmunds, C. Ferrie, R. Blatt, P. Schindler, T. Monz, R. Kueng, and M. Ringbauer, Experimental single-setting quantum state tomography, PRX Quantum **3**, 040310 (2022).

[4] R. J. MacDonell, C. E. Dickerson, C. J. T. Birch, A. Kumar, C. L. Edmunds, M. J. Biercuk, C. Hempel, and I. Kassal, Analog quantum simulation of chemical dynamics, Chem. Sci. **12**, 9794 (2021).

[5] M. Ringbauer, T. R. Bromley, M. Cianciaruso, L. Lami, W. Y. S. Lau, G. Adesso, A. G. White, A. Fedrizzi, and M. Piani, Certification and quantification of multilevel quantum coherence, Phys. Rev. X **8**, 041007 (2018).

[6] T. Kraft, C. Ritz, N. Brunner, M. Huber, and O. Gühne, Characterizing genuine multilevel entanglement, Phys. Rev. Lett. **120**, 060502 (2018).

[7] D. Cozzolino, B. Da Lio, D. Bacco, and L. K. Oxenløwe, High-dimensional quantum communication: Benefits, progress, and future challenges, Adv. Quantum Technol. **2** (2019).

[8] E. T. Campbell, Enhanced fault-tolerant quantum computing in d-level systems, Phys. Rev. Lett. **113**, 230501 (2014).

[9] A. Morvan, V. V. Ramasesh, M. S. Blok, J. M. Kreikebaum, K. O'Brien, L. Chen, B. K. Mitchell, R. K. Naik, D. I. Santiago, and I. Siddiqi, Qutrit randomized benchmarking, Phys. Rev. Lett. **126**, 210504 (2021).

[10] Y. Chi, J. Huang, Z. Zhang, J. Mao, Z. Zhou, X. Chen, C. Zhai, J. Bao, T. Dai, H. Yuan, M. Zhang, D. Dai, B. Tang, Y. Yang, Z. Li, Y. Ding, L. K. Oxenløwe, M. G. Thompson, J. L. O'Brien, Y. Li, Q. Gong, and J. Wang, A programmable qudit-based quantum processor, Nat. Commun. **13**, 1166 (2022).

[11] M. Ringbauer, M. Meth, L. Postler, R. Stricker, R. Blatt, P. Schindler, and T. Monz, A universal qudit quantum processor with trapped ions, Nat. Phys. **18**, 1053 (2022).

[12] D. Bruß, Optimal eavesdropping in quantum cryptography with six states, Phys. Rev. Lett. **81**, 3018 (1998).

[13] R. T. Thew, A. Acín, H. Zbinden, and N. Gisin, Bell-type test of energy-time entangled qutrits, Phys. Rev. Lett. **93**, 010503 (2004).

[14] P. Hauke, F. M. Cucchietti, L. Tagliacozzo, I. Deutsch, and M. Lewenstein, Can one trust quantum simulators?, Rep. Prog. Phys. **75**, 082401 (2012).

[15] J. Preskill, Quantum computing in the NISQ era and beyond, Quantum **2**, 79 (2018).

[16] K. Bharti, A. Cervera-Lierta, T. H. Kyaw, T. Haug,

S. Alperin-Lea, A. Anand, M. Degroote, H. Heimonen, J. S. Kottmann, T. Menke, W.-K. Mok, S. Sim, L.-C. Kwek, and A. Aspuru-Guzik, Noisy intermediate-scale quantum algorithms, Rev. Mod. Phys. **94**, 015004 (2022).

[17] H. B. Callen and T. A. Welton, Irreversibility and generalized noise, Phys. Rev. **83**, 34 (1951).

[18] R. Kubo, Statistical-mechanical theory of irreversible processes. i. general theory and simple applications to magnetic and conduction problems, JPSJ **12**, 570 (1957).

[19] R. Kubo, The fluctuation-dissipation theorem, Rep. Prog. Phys. **29**, 255 (1966).

[20] L. Foini, L. F. Cugliandolo, and A. Gambassi, Fluctuation-dissipation relations and critical quenches in the transverse field ising chain, Phys. Rev. B **84**, 212404 (2011).

[21] L. Foini, L. F. Cugliandolo, and A. Gambassi, Dynamic correlations, fluctuation-dissipation relations, and effective temperatures after a quantum quench of the transverse field ising chain, J. Stat. Mech. **2012**, P09011 (2012).

[22] E. Khatami, G. Pupillo, M. Srednicki, and M. Rigol, Fluctuation-dissipation theorem in an isolated system of quantum dipolar bosons after a quench, Phys. Rev. Lett. **111**, 050403 (2013).

[23] A. Piñeiro Orioli and J. Berges, Breaking the fluctuation-dissipation relation by universal transport processes, Phys. Rev. Lett. **122**, 150401 (2019).

[24] A. Schuckert and M. Knap, Probing eigenstate thermalization in quantum simulators via fluctuation-dissipation relations, Phys. Rev. Res. **2**, 043315 (2020).

[25] K. T. Geier and P. Hauke, From non-Hermitian linear response to dynamical correlations and fluctuation-dissipation relations in quantum many-body systems, PRX Quantum **3**, 030308 (2022).

[26] J. M. Deutsch, Quantum statistical mechanics in a closed system, Phys. Rev. A **43**, 2046 (1991).

[27] M. Srednicki, Chaos and quantum thermalization, Phys. Rev. E **50**, 888 (1994).

[28] R. Nandkishore and D. A. Huse, Many-body localization and thermalization in quantum statistical mechanics, Annu. Rev. Condens. Matter Phys. **6**, 15 (2015).

[29] C. Gogolin and J. Eisert, Equilibration, thermalisation, and the emergence of statistical mechanics in closed quantum systems, Rep. Prog. Phys. **79**, 056001 (2016).

[30] L. D'Alessio, Y. Kafri, A. Polkovnikov, and M. Rigol, From quantum chaos and eigenstate thermalization to statistical mechanics and thermodynamics, Adv. Phys. **65**, 239–362 (2016).

[31] J. M. Deutsch, Eigenstate thermalization hypothesis, Rep. Prog. Phys. **81**, 082001 (2018).

[32] D. A. Abanin, E. Altman, I. Bloch, and M. Serbyn, Colloquium: Many-body localization, thermalization, and entanglement, Rev. Mod. Phys. **91**, 021001 (2019).

[33] S. Moudgalya, B. A. Bernevig, and N. Regnault, Quantum many-body scars and Hilbert space fragmentation: a review of exact results, Rep. Prog. Phys. **85**, 086501 (2022).

[34] P. Sierant, M. Lewenstein, A. Scardicchio, L. Vidmar, and J. Zakrzewski, Many-body localization in the age of classical computing (2024), arXiv:2403.07111 [cond-mat.dis-nn].

[35] M. Cerezo, A. Arrasmith, R. Babbush, S. C. Benjamin, S. Endo, K. Fujii, J. R. McClean, K. Mitarai, X. Yuan, L. Cincio, and P. J. Coles, Variational quantum algo-rithms, Nat. Rev. Phys. **3**, 625–644 (2021).

[36] J. Tilly, H. Chen, S. Cao, D. Picozzi, K. Setia, Y. Li, E. Grant, L. Wossnig, I. Rungger, G. H. Booth, and J. Tennyson, The variational quantum eigensolver: A review of methods and best practices, Phys. Rep. **986**, 1 (2022).

[37] D. Wierichs, J. Izaac, C. Wang, and C. Y.-Y. Lin, General parameter-shift rules for quantum gradients, Quantum **6**, 677 (2022).

[38] Y. Li and S. C. Benjamin, Efficient variational quantum simulator incorporating active error minimization, Phys. Rev. X **7**, 021050 (2017).

[39] S. McArdle, T. Jones, S. Endo, Y. Li, S. C. Benjamin, and X. Yuan, Variational ansatz-based quantum simulation of imaginary time evolution, Npj Quantum Inf. **5** (2019).

[40] X. Yuan, S. Endo, Q. Zhao, Y. Li, and S. C. Benjamin, Theory of variational quantum simulation, Quantum **3**, 191 (2019).

[41] P. P. Popov, M. Meth, M. Lewestein, P. Hauke, M. Ringbauer, E. Zohar, and V. Kasper, Variational quantum simulation of U(1) lattice gauge theories with qudit systems, Phys. Rev. Res. **6**, 013202 (2024).

[42] M. Knap, A. Kantian, T. Giamarchi, I. Bloch, M. D. Lukin, and E. Demler, Probing real-space and time-resolved correlation functions with many-body Ramsey interferometry, Phys. Rev. Lett. **111**, 147205 (2013).

[43] N. Y. Yao, F. Grusdt, B. Swingle, M. D. Lukin, D. M. Stamper-Kurn, J. E. Moore, and E. A. Demler, Interferometric approach to probing fast scrambling (2016), arXiv:1607.01801 [quant-ph].

[44] P. Uhrich, S. Castrignano, H. Uys, and M. Kastner, Non-invasive measurement of dynamic correlation functions, Phys. Rev. A **96**, 022127 (2017).

[45] A. Elben, B. Vermersch, M. Dalmonte, J. Cirac, and P. Zoller, Renyi entropies from random quenches in atomic Hubbard and spin models, Phys. Rev. Lett. **120**, 50406 (2018).

[46] B. Vermersch, A. Elben, L. M. Sieberer, N. Y. Yao, and P. Zoller, Probing scrambling using statistical correlations between randomized measurements, Phys. Rev. X **9**, 021061 (2019).

[47] A. K. Ekert, C. M. Alves, D. K. L. Oi, M. Horodecki, P. Horodecki, and L. C. Kwek, Direct estimations of linear and nonlinear functionals of a quantum state, Phys. Rev. Lett. **88**, 217901 (2002).

[48] B. Bauer, D. Wecker, A. J. Millis, M. B. Hastings, and M. Troyer, Hybrid quantum-classical approach to correlated materials, Phys. Rev. X **6**, 031045 (2016).

[49] K. Mitarai and K. Fujii, Methodology for replacing indirect measurements with direct measurements, Phys. Rev. Res. **1**, 013006 (2019).

[50] W. J. Huggins, K. Wan, J. McClean, T. E. O'Brien, N. Wiebe, and R. Babbush, Nearly optimal quantum algorithm for estimating multiple expectation values, Phys. Rev. Lett. **129**, 240501 (2022).

[51] F. Libbi, J. Rizzo, F. Tacchino, N. Marzari, and I. Tavernelli, Effective calculation of the Green's function in the time domain on near-term quantum processors, Phys. Rev. Res. **4**, 043038 (2022).

[52] A. Baroni, J. Carlson, R. Gupta, A. C. Y. Li, G. N. Perdue, and A. Roggero, Nuclear two point correlation functions on a quantum computer, Phys. Rev. D **105**, 074503 (2022).

[53] N. Mueller, J. A. Carolan, A. Connelly, Z. Davoudi, E. F. Dumitrescu, and K. Yeter-Aydeniz, Quantum computation of dynamical quantum phase transitions and entanglement tomography in a lattice gauge theory, PRX Quantum **4**, 030323 (2023).

[54] S. Chakraborty, Implementing any linear combination of unitaries on intermediate-term quantum computers (2024), arXiv:2302.13555 [quant-ph].

[55] C. Monroe, W. C. Campbell, L.-M. Duan, Z.-X. Gong, A. V. Gorshkov, P. W. Hess, R. Islam, K. Kim, N. M. Linke, G. Pagano, P. Richerme, C. Senko, and N. Y. Yao, Programmable quantum simulations of spin systems with trapped ions, Rev. Mod. Phys. **93**, 025001 (2021).

[56] C. L. Edmunds, E. Rico, I. Arrazola, G. K. Brennen, M. Meth, R. Blatt, and M. Ringbauer, Constructing the spin-1 haldane phase on a qudit quantum processor (2024), arXiv:2408.04702 [quant-ph].

[57] F. Haldane, Continuum dynamics of the 1-d heisenberg antiferromagnet: Identification with the o(3) nonlinear sigma model, Physics Letters A **93**, 464 (1983).

[58] F. D. M. Haldane, Nonlinear field theory of large-spin heisenberg antiferromagnets: Semiclassically quantized solitons of the one-dimensional easy-axis néel state, Phys. Rev. Lett. **50**, 1153 (1983).

[59] W. Chen, K. Hida, and B. C. Sanctuary, Ground-state phase diagram of $s = 1$ XXZ chains with uniaxial single-ion-type anisotropy, Phys. Rev. B **67**, 104401 (2003).

[60] J. Berges, 69nonequilibrium quantum fields: from cold atoms to cosmology, in *Strongly Interacting Quantum Systems out of Equilibrium: Lecture Notes of the Les Houches Summer School: Volume 99, August 2012* (Oxford University Press, 2016).

[61] M. Meth, J. F. Haase, J. Zhang, C. Edmunds, L. Postler, A. Steiner, A. J. Jena, L. Dellantonio, R. Blatt, P. Zoller, T. Monz, P. Schindler, C. Muschik, and M. Ringbauer, Simulating 2D lattice gauge theories on a qudit quantum computer (2024), arXiv:2310.12110 [quant-ph].

[62] L. Pan, X. Chen, Y. Chen, and H. Zhai, Non-Hermitian linear response theory, Nat. Phys. **16**, 767 (2020).

[63] D. Sticlet, B. Dóra, and C. P. Moca, Kubo formula for non-Hermitian systems and tachyon optical conductivity, Phys. Rev. Lett. **128**, 016802 (2022).

[64] In the non-Hermitian case, we reduce the number of shots according to the decrease of the norm of the state.

[65] Z.-Y. Zhou, G.-X. Su, J. C. Halimeh, R. Ott, H. Sun, P. Hauke, B. Yang, Z.-S. Yuan, J. Berges, and J.-W. Pan, Thermalization dynamics of a gauge theory on a quantum simulator, Science **377**, 311–314 (2022).

[66] P. P. Popov, K. T. Geier, V. Kasper, M. Lewenstein, and P. Hauke, Qudit-native measurement protocol for dynamical correlations using hadamard tests [Data set], 10.5281/zenodo.15089902 (2025).

[67] S. Polla, G.-L. R. Anselmetti, and T. E. O'Brien, Optimizing the information extracted by a single qubit measurement, Phys. Rev. A **108**, 012403 (2023).